

Properties of ABS/Organic-Attapulgite Nanocomposites Parts Fabricated by Fused Deposition Modeling

Ling Wang^{1,2}, Shenglong Jiang², Chenchen Huang², Pengyuan Dai², Fenghua Liu^{2,*}, Xiaopeng Qi¹ and Gaojie Xu²

¹Faculty of Materials Metallurgy and Chemistry, Jiangxi University of Science and Technology, Ganzhou, 341000, China

²Key Laboratory of Additive Manufacturing Materials of Zhejiang Province, Ningbo Institute of Materials Technology and Engineering, Chinese Academy of Science, Ningbo, 315201, China

*Corresponding Author: Fenghua Liu. Email: lfh@nimte.ac.cn

Received: 17 April 2020; Accepted: 26 May 2020

Abstract: The paper discusses the mechanical and thermal performance manifested in natural nanorods attapulgite (ATP) reinforced Acrylonitrile butadiene styrene (ABS) nanocomposites in the process of fused deposition modeling (FDM). Molten extrusion technique was taken to manufacture the filaments of ABS/organic-attapulgite (OAT) nanocomposites with different mass fraction and the printing operation was made by one commercial FDM three-dimensional (3D) printer. Results indicate that the mechanical performance of these FDM 3D printed specimens are improved obviously via the introduction of OAT, and tensile strength of the ABS/OAT nanocomposites parts with only 2 wt% OAT addition is enhanced by 48.1%. At the same time, the addition OAT can reduce the linear expansion coefficient and creep flexibility, and improve the thermal stability and dimensional accuracy of these FDM 3D printed parts.

Keywords: ABS; organic-attapulgite; fused deposition modeling; nanocomposites

1 Introduction

By far, additive manufacturing (AM) has been taken as a focus of attention across the industrial circles and academic circles as a result of its capacity of manufacturing sophisticated and bespoke components, and also prominent edge in less time consumption [1–4]. Fused deposition modelling (FDM), as a commonplace AM method, exhibits irreplaceable superiority in respect of easy operation, low cost of maintenance, unsupervised operation, as well as small volume [5–7]. Representative FDM process extrudes the filament of thermoplastic materials at a preset temperature greater than glass transition temperature or melting temperature via the nozzle, and then tridimensional (3D) objects take shape after the filament permeates into the platform layer by layer. Whereas, there are just few types of thermoplastic materials that can be applied in FDM for the preparation of filaments, such as acrylonitrile butadiene styrene (ABS) [7–9], polylactide (PLA) [10,11], polyamide (PA) [12] and so forth. Another point worth mentioning is that as such pure thermoplastic printed components remain defective in mechanical strength, their scope of application has been greatly prohibited.



This work is licensed under a Creative Commons Attribution 4.0 International License, which permits unrestricted use, distribution, and reproduction in any medium, provided the original work is properly cited.

One of the effective means of improving FDM parts' mechanical performance is to develop polymer matrix compounds [13–16]. Due to its excellent performance in optimizing host matrices with a fraction of filler, polymer nanocomposites (PNCs) has held widespread attention recently [17–20]. The addition of nanomaterials, in particular one-dimensional nanomaterials represented by carbon nanotubes and nanowires, to matrices by virtue of AM may ameliorate the properties of obtained parts [21–23]. Attapulgite (ATP) refers to sort of inartificial 1D nano-scale hydrous aluminosilicate silicate clay mineral rich in magnesium. It is often in a 2:1 layer-chain microstructure, featuring a crystal form patterned after nanorod, conventional nanopores, as well as active surface silanol perssads [24–26]. Combined with the distinctive composition of nanorod crystals and nanopores, it possesses wider surface coverage, greater mechanical intensity, high aspect ratio, as well as superb thermal stability [27,28]. Compared with the synthetic 1D nano-scale materials such as carbon nanotubes and nanowires, the natural ATP nanorods have adjustable surface chemistry and low cost, which makes it have a good application prospect in the field of composite materials. According to the literature review, few dissertations concerning polymer matrix issued on scientific journals introduce ATP into FDM as nanofillers.

In the present study, the filaments of ABS/organic-attapulgite (OAT) nanocomposites with different mass fraction had been manufactured for the application in FDM by molten extrusion technique, and printed as various test samples. Differential scanning calorimetry (DSC) and dynamic mechanical thermal analysis (DMA) had been taken in the analysis to depict the thermal performance of the composites. Sample mechanical performance was represented by the three point bending experiments and tensile experiments. As indicated by the research results, the introduction of OAT greatly improved the thermal-mechanical performance of ABS/OAT nanocomposites. Subsequently, the paper adopted SEM to investigate ATP's distribution and orientation in composite carbides and also the interface between ATP and thermoplastic matrix.

2 Experimental

2.1 Materials

Phenyltrimethoxysilane coupling agent KH-162, ethanol (EtOH), hydrochloric acid (37%, AR) were provided by the Chinese company Sinopharm Chemical Reagent Co., Ltd., Deionized water of 18.3 MΩ cm resistivity came from the Millipore Milli-Q System, the raw ABS pellets was supplied by the Chinese company Qimei Stock Company, and the pristine attapulgite (ATP) was procured from Jiangsu Jiuchuan Material Technology Co., Ltd.

2.2 Preparation of Organic-Attapulgite Power

Firstly, the attapulgite was acid activated by immersing the powder in 0.5 mol/L HCl at 80°C for 1 h, followed by washing with deionized water and ethanol, and then drying in a 120°C oven. The lump-shaped ATP solids were ground, then through 500 mesh sieving, and the ATP powder was obtained. The ATP powder was dissolved in toluene, with the addition of silane as coupling agent. After ultrasonic stirring for 50 m, followed by coupling reaction, heating, and mechanical stirring reaction at 100°C for 10 h. The liquid was added to suction filtration, then washed many times with toluene, deionized water and ethanol. After filtrated and dried for over 12 hours, followed by sieving through 500 mesh, and Organic-ATP powder was obtained.

2.3 Preparation of ABS/Organic-Attapulgite Nanocomposites

Firstly, ABS particles and different amount of organic-attapulgite (OAT) powders (1 wt%, 2 wt%, 3 wt%, 5 wt% of ABS particles) were physically mixed by V-type mixer. After that, a twin-screw extruder in 20 mm diameter with 40 L/D ratio and 20/40 KEDSE developed by the German manufacturer Brabender® GmbH & Co., KG was reported to extrude the molten mixture of ABS and OAT. **Tab. 1** presents parameters involved in the operation of the twin screw extruder. Extruded ABS/OAT nanocomposites would be pelletized and treated by vacuum oven-drying at 80°C for 4 h.

Table 1: Operation parameters for the application of twin-screw extruder

Extruder section	Z1	Z2	Z3	Z4	Z5	Die
Temperature (°C)	225	230	230	225	225	215
Rate of screw (rpm)	40					
Torque of screw (N·m)	30					

2.4 Filaments Extrusion of ABS/Organic-Attapulgite Nanocomposites

The filaments of ABS/organic-attapulgite (OAT) nanocomposites with a diameter of 1.75 ± 0.05 mm were fabricated by the filament production kit SHSJ-35 procured from the Chinese company Songhu Plastic Machinery Co., Ltd., including one single-screw extruder with 35 mm diameter and 25 L/D ratio, two water tanks, and also one pulling and take-up unit. Tab. 2 lists the parameters of operation in filament manufacturing process.

Table 2: Operation parameters for the preparation of filament

Extruder section	Z1	Z2	Z3	Z4	Z5	Die
Temperature (°C)	215	220	220	215	215	205
Rate of screw (rpm)	60					
Temperature in Water tank (°C)	60 (tank 1)			40 (tank 2)		
Rate of pulling speed (cm/s)	30					

2.5 The FDM Process of ABS/Organic-Attapulgite Filaments

The preparation of ABS/organic-attapulgite filaments was made by one commercial FDM printer (JGAURORA A8 3-D printer, Jgaurora Technology Co., Ltd., China). In printing operation, the temperature of printing nozzle and hot bed was set to be 240°C and 60°C. Specimens were straightforward marked on support-free heating plates. The layer thickness, printing speed and infilling rate of all samples were set as 0.2 mm, 60 mm/s and 100%, respectively.

2.6 Characterization of Nanocomposites

The chemical structure of ATP and OAT was determined by an intelligent Fourier transform Infrared spectrometer (Nicolet 6700) in which the IR spectra was recorded by diluting the milled powders in KBr. Field-emission scanning electron microscope Hitachi S4800 was chosen as the apparatus in the experiment used for observing specimen morphology and microstructure. Dimond DSC (PerkinElmer, USA) was adopted to characterize ABS/OAT specimens' glass-transition temperature in the nitrogen environment. The thermo-stability behavior of the ABS/OAT samples was characterized via Dimond TG/DTA (PerkinElmer, USA), in which the rate of heating was set as 10°C/min and corresponding scope of temperature varied between room temperature and 800°C under an air atmosphere. Measurement about the interplay between the ABS and OAT interface in printed specimens ($25 \times 5 \times 1.5$ mm) had been realized by DMA-Q800 (TA, USA) under the tensile mode. Samples then went through heating treatment at -100°C – 150°C with the speed of 3°C/min at 1 Hz. While the measurement about the linear thermo expansion ratio of ABS/OAT specimens was performed by the thermal dilatometer DIL402C developed by NETZSCH in Germany. During the test, the primary length of specimens was set as 12 mm and corresponding scope of temperature varied between 25°C and 80°C.

3 Results and Discussion

3.1 Modification and Dispersion of ATP

As shown in Fig. 1, the organic-ATP (OAT) powder was obtained after a series of steps.

The FT-IR spectra of ATP and modified ATP are shown in Fig. 2. As shown in Fig. 2, the adsorption bands at 3614.77, 3551.26 and 1654.72 cm^{-1} should be triggered by the $-\text{OH}$ stretching and bending shock of ATP, and adsorption bands at 1028.26 and 984.82 cm^{-1} should be triggered by the *asymmetric* stretching shock of $\text{Si}-\text{O}-\text{Si}$ and bending shock of $\text{O}-\text{H}$ in ATP. After acidification, there are no new adsorption bands appeared. However, after modification with KH-162, some new adsorption bands at 1430.84 and 738.95, 697.98 cm^{-1} were appeared in the spectrum of OAT which should be triggered by the $\text{C}=\text{C}$ stretching shock of benzene ring and $\text{C}-\text{H}$ bending shock in benzene ring respectively, that means KH-162 was successfully grafted on ATP.

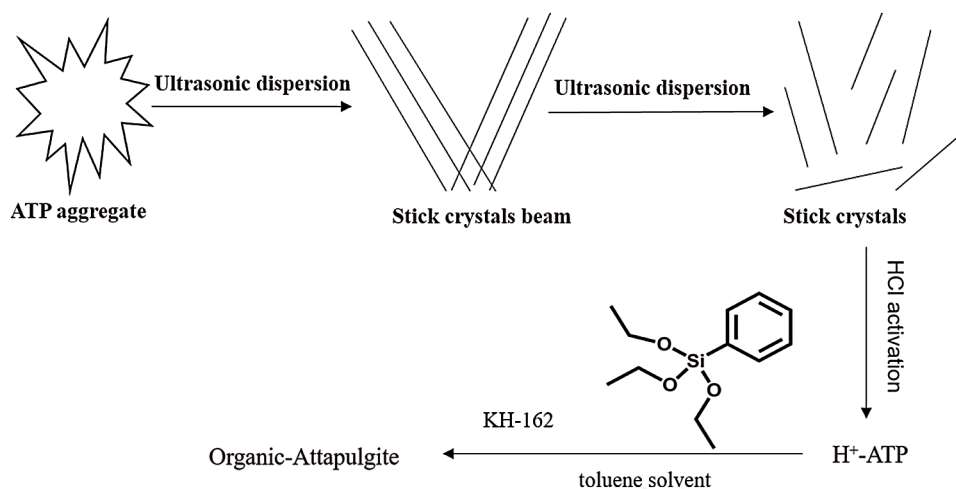


Figure 1: The preparation scheme of organic-ATP powder

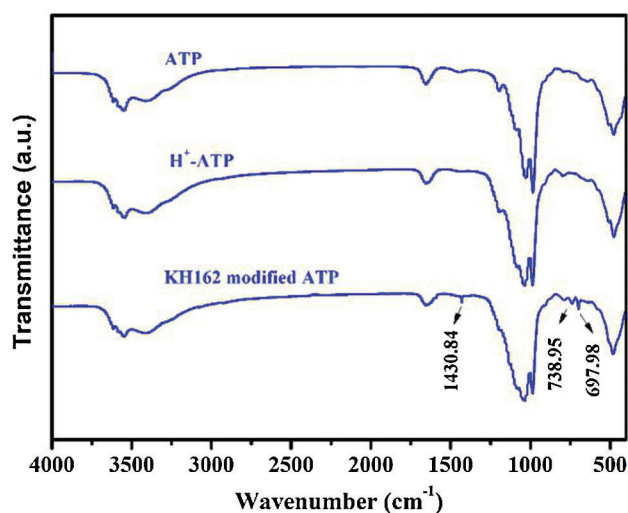


Figure 2: FTIR spectra of raw ATP, acid activated ATP and KH-162 modified ATP

The SEM images of raw ATP and KH-162 modified ATP are shown in Figs. 3a and 3b. As shown in Fig. 3a, the diameter and length of the raw ATP is about 30–50 nm and 0.5–1.0 μm respectively. Evidence also shows the intensiveness and compactness of the material. Tested ATP fibers either flat or straight in shape are in random orientation in aggregates. After modification with KH-162, OAT improved by KH-162 demonstrates a well-organized and discrete structure.

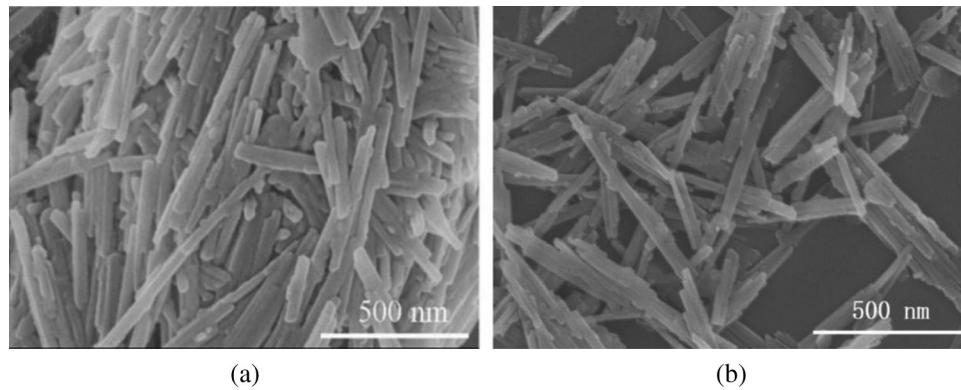


Figure 3: SEM images of (a) raw ATP, (b) KH-162 modified ATP

The representative SEM micrographs of ABS/OAT composites with different amount of OAT are shown in Fig. 4. From Fig. 4 we can see many uniform light dots with the diameters 100–200 nm in the images of ABS/OAT (1 and 2 wt%) composites. The uniform white dot indicates that the OAT is well dispersed in the matrix ABS and forms the insertion structure. Fig. 4 also shows that there are slight and large-scale rods which may form aggregates in the ABS/OAT (3 wt%) and ABS/OAT(5 wt%) composites, respectively. Under the theory of Griffith, large aggregate seems to be a vulnerable spot detrimental to the reinforcement of composite stress [29].

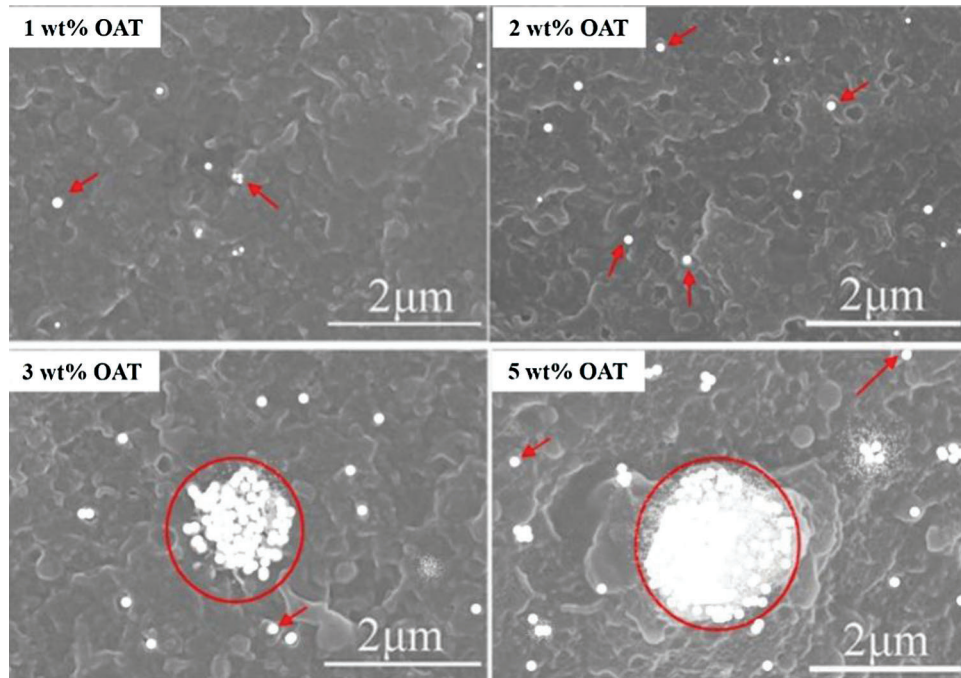


Figure 4: SEM micrographs of ABS/OAT (1, 2, 3, 5 wt%) composites

3.2 Microstructure of the 3D Printed ABS/OAT Nanocomposites

As shown in Fig. 5, it can be seen that the gap and space between adjacent filaments are obviously smaller when OAT was introduced to ABS matrix. In general, the smaller the gap between the layers, the denser the printed specimens and the better mechanical performances [30]. This was also confirmed by the results from mechanical property study.

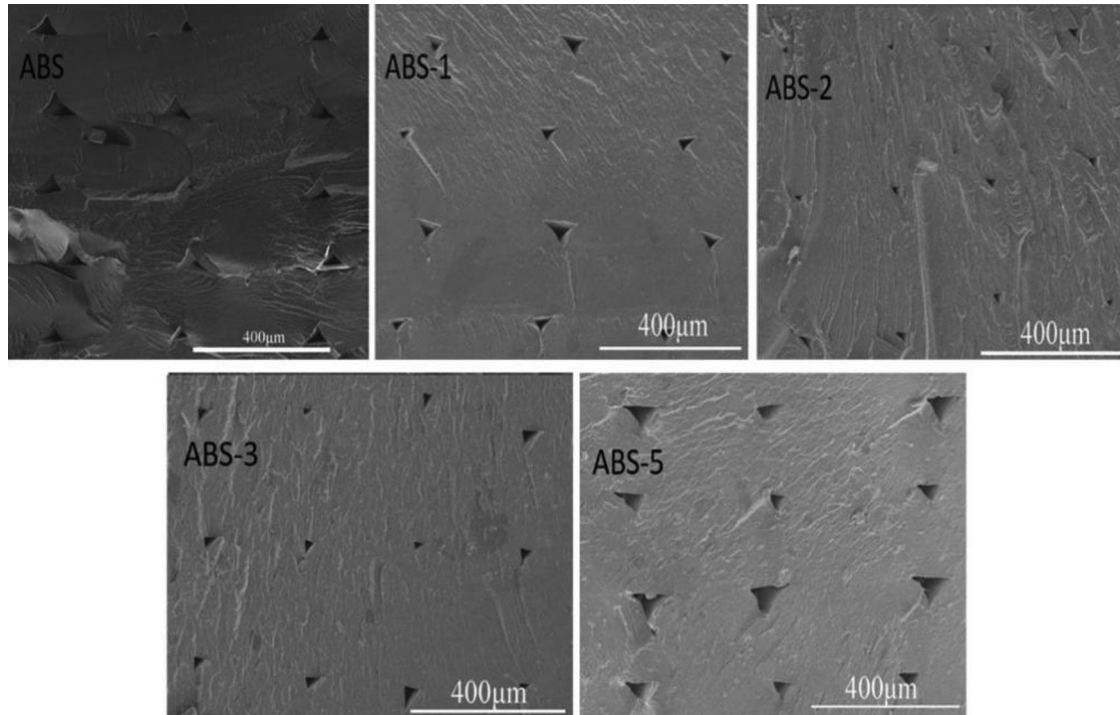


Figure 5: SEM micrographs of the fracture surface of 3D printed 0° ABS/OAT (0, 1, 2, 3, 5 wt%) nanocomposites specimens

As shown in Fig. 6, in the 3D printing operation of FDM application, the arrangement of OAT is aligned with the extrusion orientation, but during compression moulded, the OAT is randomly arranged. The orientated OAT has superior performance following the direction of the filament.

3.3 Mechanical Properties

Mechanical properties of ABS/OAT nanocomposite components produced with 3D printer have been listed as shown in Tab. 3 and Fig. 7. As proved by the results, the addition of 1 wt% OAT significantly improves the tensile strength and other mechanical performance of FDM 3D printed specimens. The tensile strength and flexural strength reached a maximum value when the OAT content is 2 wt%. Compared with the pure ABS, the tensile strength, elastic modulus and flexural strength of the ABS/OAT nanocomposites parts with only 2 wt% OAT addition are enhanced by 48.1%, 25.5% and 4.8% respectively.

3.4 Thermal Properties

The typical TG and DTG curves of ABS and ABS/OAT nanocomposites have been listed in Fig. 8. A major phase of weight loss was observed in the range of 350 to 500°C, which was due to the structural decomposition of the ABS matrix. Compared with the pure ABS, the thermal decomposition starting temperature (T_m) of ABS/OAT nanocomposites are enhanced. The improvement of thermal stability can be attributed to the mass transfer barrier of OAT to volatile products during ABS decomposition.

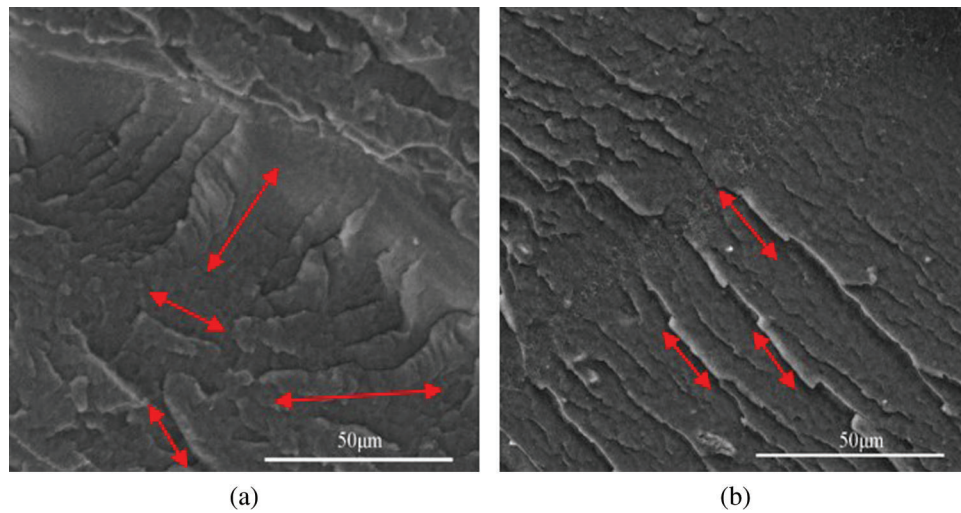


Figure 6: SEM images of the fracture surface of compression moulded (a) and printed (b) ABS/OAT (2 wt%) nanocomposites specimens

Table 3: Mechanical properties of ABS/OAT samples by FDM

Samples	Elastic modulus (MPa)	Tensile strength (MPa)	Flexural strength (MPa)	Flexural modulus (MPa)
ABS	1910 ± 36	26 ± 2	56 ± 0.7	2110 ± 125
ABS/1%OAT	2163 ± 25	37.3 ± 0.4	57 ± 1.2	2056 ± 282
ABS/2%OAT	2398 ± 26	38.5 ± 0.5	58.7 ± 0.8	1967 ± 159
ABS/3%OAT	2244 ± 55	35.5 ± 2	57.5 ± 0.2	2091 ± 55
ABS/5%OAT	2421 ± 60	33.6 ± 0.7	58.5 ± 0.5	2248 ± 66

The DSC curves of ABS and ABS/OAT samples have been listed in Fig. 9. Results suggest that the glass transition temperature (T_g) of ABS/OAT is higher than that of pure ABS, and increases with the increase of OAT content. When the added amount of OAT increases to 5 wt%, the T_g value increases from 100°C to 110°C. Thus it can be seen that OAT has a great potential in improving the thermal performance of ABS/OAT Specimens.

3.5 Dynamic Mechanical Analysis and Coefficient of Thermal Expansion

An analysis has been carried out on the dynamic mechanical performance of ABS and ABS/OAT specimens in the horizontal direction of FDM 3D printing (Fig. 10). Tab. 4 summarizes the chosen value of storage modulus (E'), loss modulus (E''), as well as temperature in glass transition of loss tangent ($\tan \delta$). In condition of low temperature (-50°C), the addition of 3 wt% OAT to the ABS matrix promotes the storage modulus of FDM components by 9% in comparison with that of pure ABS. This is in particular true of the addition of 5 wt% OAT nanorods. In condition of high temperature, say 115°C, the storage modulus of ABS/5 wt% OAT is twice more than the value in pure ABS, which implies that molten OAT nanorods exert positive stiffening effect as shown in Tab. 4.

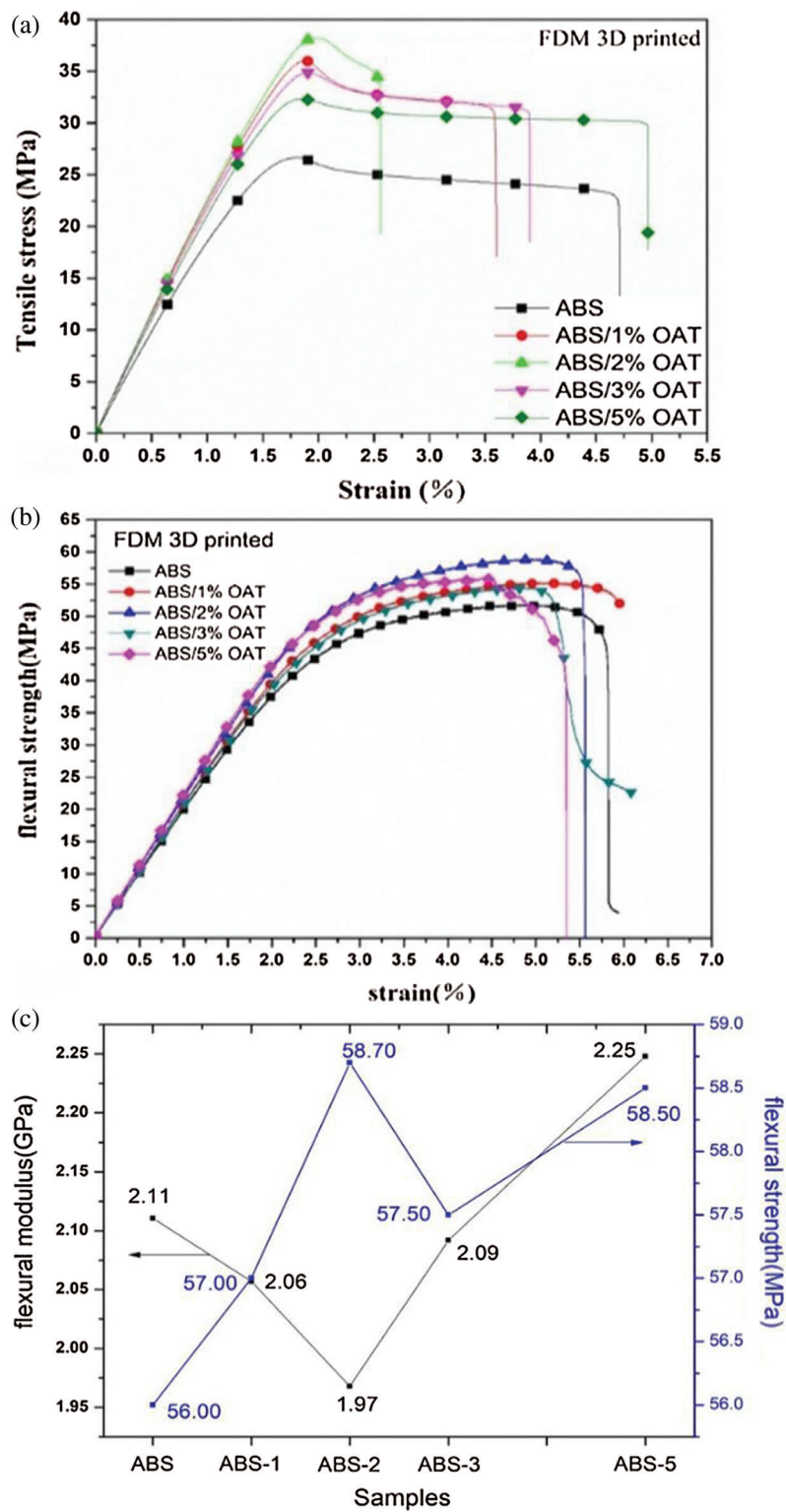


Figure 7: Tensile strength (a), flexural strength (b) and flexural modulus (c) of ABS/OAT (0, 1, 2, 3, 5 wt%) nanocomposites specimens prepared with FDM 3D printer

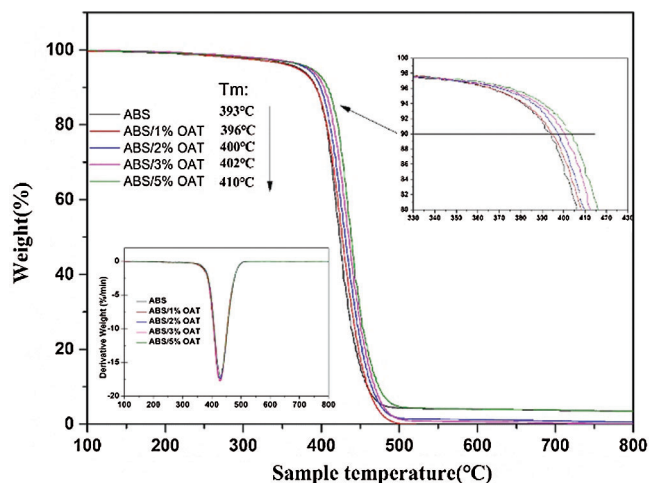


Figure 8: TG and DTG curves of ABS/OAT(0, 1, 2, 3, 5 wt%) samples

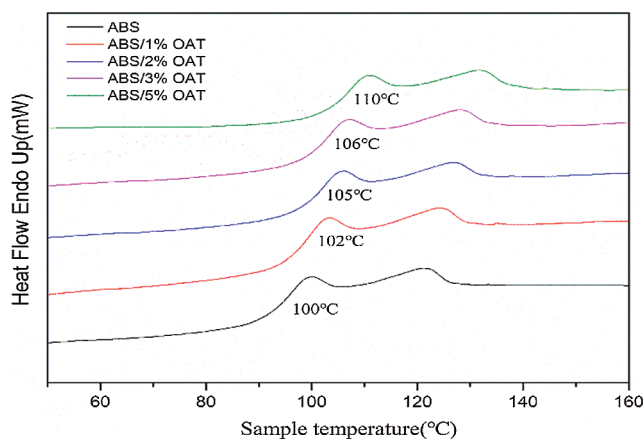


Figure 9: DSC curves of ABS and ABS/OAT (1, 2, 3, 5 wt%) samples

According to the experimental results for Loss tangent ($\tan \delta$), there are two damping peaks in ABS copolymers as shown in Fig. 10, in which the first peak rises at around -74°C associated with the glass transition temperature (T_{g1}) butadiene rich phase [31], and the second transition (T_{g2}) occurs at around 114°C associated with the styrene–acrylonitrile (SAN) rich phase. Owing to the availability of OAT, the experiment sees a rise in T_{g2} values owing to the limited mobility of macromolecules. The introduction of OAT leads to the growth of storage modulus compared with neat ABS. Under room temperature conditions, rise of storage modulus by 2.8%, 1.2% and 7% is accompanied by the addition of 1 wt%, 2 wt% and 3 wt% OAT in succession. It means that the drop of storage modulus begins with the addition of 5 wt% OAT.

And more notably, glass-rubbery transition damping peak in ABS fluctuates from 100 to 124°C [32–34]. This is totally decided by a series of considerations, like copolymer composition, molecular weight, additives, etc. Likewise, due to the availability of OAT, the addition of 5 wt% OAT simultaneously leads to a minor change of loss modulus (E'') peak temperature by 4.5 degrees. The insignificant expansion of the width of loss modulus peak in OAT/ABS composites reveals constraints in polymer chain. The reason possibly lies in the fact that the chain mobility of SAN rubber phase enclosed by OAT nanorods has met with restriction.

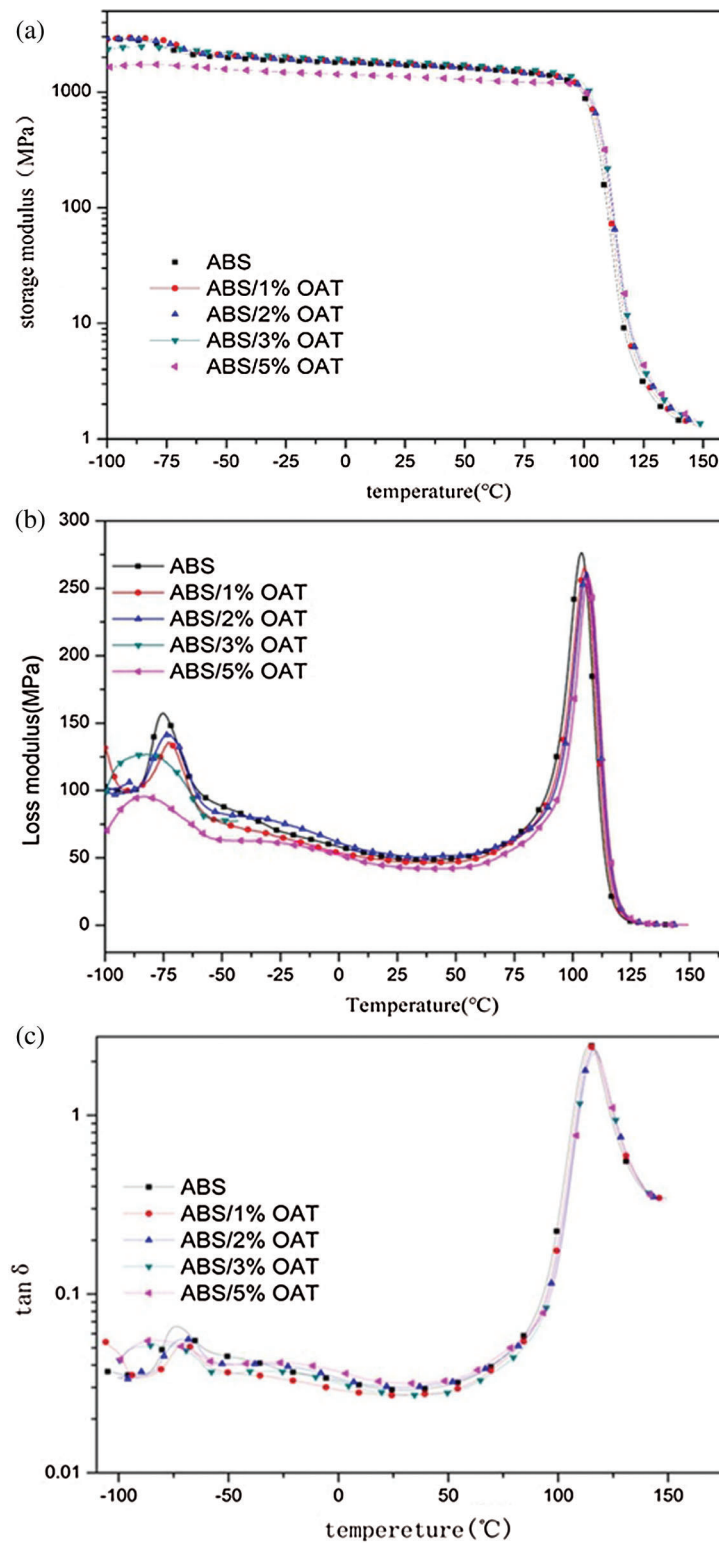


Figure 10: Dynamic mechanical analysis (a) storage modulus (E'), (b) loss modulus (E'') and loss tangent ($\tan \delta$) of ABS and ABS/OAT samples formed along the horizontal direction by FDM 3D printing

Table 4: Dynamic mechanical performance of ABS and ABS/OAT samples formed along the horizontal direction by FDM 3D printing

Samples	Storage modulus			Damping peaks		Loss modulus of SAN peak		
	-50°C (MPa)	30°C (MPa)	115°C (MPa)	B-phase T_{g1} (°C)	SAN-phase T_{g2} (°C)	E''_{peak} (MPa)	T_{peak} (°C)	W_{peak}^a (°C)
ABS	1978	1678	14	-73.8	114.2	274	104.1	13
ABS/1%OAT	2086	1725	21	-69.9	115.6	264	105.3	14
ABS/2%OAT	2047	1699	28.7	-69.0	116.4	262	106.2	13
ABS/3%OAT	2165	1796	31.2	-78.9	116.3	277	106.0	12.8
ABS/5%OAT	1574	1343	37.2	-85.2	116.6	257	108.6	12.6

^a Width at half peak.

The thermal expansion coefficient of material is the key factor to affect the dimensional accuracy of FDM forming samples. In the process of FDM 3D printing, the size of materials with low thermal expansion coefficient generally does not change significantly with the change of temperature, so the formed samples have high dimensional accuracy. Coefficient of thermal expansion in pure ABS and ABS/OAT samples are shown in Fig. 11 and the corresponding linear expansion coefficient values are listed in Tab. 5. The results show a linear downward trend of OAT thermo expansion ratio which is accompanied by the growth of content. This indicates that the OAT plays a role in limiting polymer chain mobility and decreasing linear contraction. As a consequence, adding OAT to ABS matrix has the potential of diminishing the deformation probability of FDM 3D printing parts and maintain the dimensional integrity of parts.

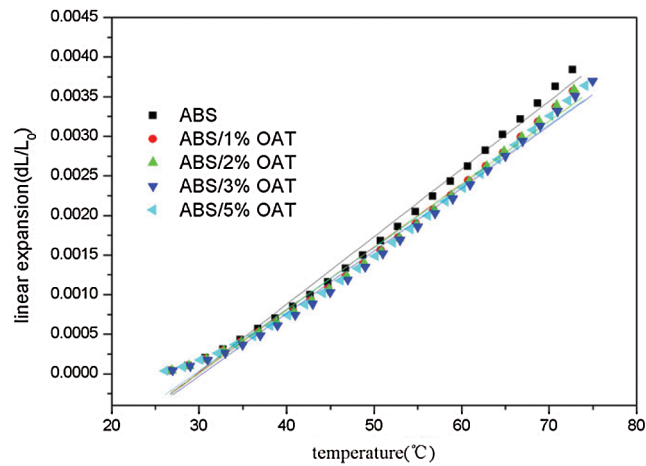
**Figure 11:** Coefficient of thermal expansion of pure ABS and ABS/OAT specimens

Table 5: Coefficient of linear expansion in specimens

Specimens	Coefficient of linear expansion
ABS	85.5 ppm•°C ⁻¹
ABS/1%OAT	79.8 ppm•°C ⁻¹
ABS/2%OAT	79.1 ppm•°C ⁻¹
ABS/3%OAT	78.9 ppm•°C ⁻¹
ABS/5%OAT	78.5 ppm•°C ⁻¹

4 Conclusion

Printable filaments of ABS/organic-attapulgite (OAT) nanocomposites with different mass fractions had been manufactured according to the melting extrusion method and finished composites were later smoothly printed by the commercial FDM printer. Specimen mechanical performance was characterized by three point bending experiment and tensile experiment, while specimen the thermal performance was labeled by differential scanning calorimetry (DSC) and also dynamic mechanical thermal analysis (DMA) method. As proven by the findings, the introduction of OAT to ABS/OAT nanocomposites can remarkably improve the thermal and mechanical performance of the material. While tensile strength of the FDM printed ABS/OAT parts with only 2 wt% OAT addition is enhanced by 48.1%. At the same time, the addition OAT can reduce the linear expansion coefficient and creep flexibility, and improve the thermal stability and dimensional accuracy of these FDM 3D printed parts. Accordingly, introducing OAT to ABS matrix takes a great advantage in improving the comprehensive performance of FDM printed ABS nanocomposites parts. These filaments of ABS/OAT could be used as high-efficient materials suitable for FDM 3D printing.

Funding Statement: The authors gratefully acknowledge the financial support by the Jiangsu Key R & D program (BE2019072).

Conflicts of Interest: The authors declare that they have no conflicts of interest to report regarding the present study.

References

1. Ertan, R., Durgun, I. (2014). Experimental investigation of FDM process for improvement of mechanical properties and production cost. *Rapid Prototyping Journal*, 20(3), 228–235. DOI 10.1108/RPJ-10-2012-0091.
2. Ivanova, O., Williams, C., Campbell, T. (2013). Additive manufacturing (AM) and nanotechnology: promises and challenges. *Rapid Prototyping Journal*, 19(5), 353–364. DOI 10.1108/RPJ-12-2011-0127.
3. Dimitrov, D., Schreve, K., Beer, N. D. (2006). Advances in three dimensional printing—state of the art and future perspectives. *Rapid Prototyping Journal*, 12(3), 136–147. DOI 10.1108/13552540610670717.
4. Krawczak, P. (2015). Additive manufacturing of plastic and polymer composite parts: promises and challenges of 3D-printing. *Express Polymer Letters*, 9(11), 959–966. DOI 10.3144/expresspolymlett.2015.86.
5. Love, L. J., Kunc, V., Rios, O., Duty, C. E., Elliott, A. M. et al. (2014). The importance of carbon fiber to polymer additive manufacturing. *Journal of Materials Research*, 29(17), 1893–1898. DOI 10.1557/jmr.2014.212.
6. Tekinalp, H. L., Kunc, V., Velez-Garcia, G. M., Duty, C. E., Love, L. J. et al. (2014). Highly oriented carbon fiber-polymer composites via additive manufacturing. *Composites Science & Technology*, 105, 144–150. DOI 10.1016/j.compscitech.2014.10.009.
7. Perez, A. R. T., Roberson, D. A., Wicker, R. B. (2014). Fracture surface analysis of 3D-printed tensile specimens of novel ABS-based materials. *Journal of Failure Analysis & Prevention*, 14(4), 343–353. DOI 10.1007/s11668-014-9803-9.

8. Singh, J., Singh, R., Singh, H. (2016). Repeatability of linear and radial dimension of ABS rep-licas fabricated by fused deposition modelling and chemical vapor smoothing process: a case study. *Measurement*, 94, 5–11. DOI 10.1016/j.measurement.2016.07.064.
9. Weng, Z., Wang, J., Senthil, T., Wu, L. (2016). Mechanical and thermal properties of ABS/montmorillonite nanocomposites for fused deposition modeling 3D printing. *Materials & Design*, 102, 276–283. DOI 10.1016/j.matdes.2016.04.045.
10. Drummer, D., Cifuentes-Cuéllar, S., Rietzel, D. (2012). Suitability of PLA/TCP for fused deposition modeling. *Rapid Prototyping Journal*, 18(6), 500–507. DOI 10.1108/13552541211272045.
11. Prashantha, K., Roger, F. (2016). Multifunctional properties of 3D printed poly(lactic acid)/graphene nanocomposites by fused deposition modeling. *Journal of Macromolecular Science Part A*, 54(1), 24–29. DOI 10.1080/10601325.2017.1250311.
12. Zhu, D., Ren, Y., Liao, G., Jiang, S., Liu, F. et al. (2017). Thermal and mechanical properties of polyamide 12/graphene nanoplatelets nanocomposites and parts fabricated by fused deposition modeling. *Journal of Applied Polymer Science*, 134(39), 45332. DOI 10.1002/app.45332.
13. Masood, S. H., Song, W. Q. (2004). Development of new metal/polymer materials for rapid tooling using Fused Deposition Modelling. *Materials & Design*, 25(7), 587–594. DOI 10.1016/j.matdes.2004.02.009.
14. Nikzad, M., Masood, S. H., Sbarski, I. (2011). Thermo-mechanical properties of a highly filled polymeric composites for Fused Deposition Modeling. *Materials & Design*, 32(6), 3448–3456. DOI 10.1016/j.matdes.2011.01.056.
15. Shofner, M. L., Lozano, K., Rodríguez-Macías, F. J., Barrera, E. V. (2010). Nanofiber-reinforced polymers prepared by fused deposition modeling. *Journal of Applied Polymer Science*, 89(11), 3081–3090. DOI 10.1002/app.12496.
16. Zhong, W., Li, F., Zhang, Z., Song, L., Li, Z. (2001). Short fiber reinforced composites for fused deposition modeling. *Materials Science & Engineering: A*, 301(2), 125–130. DOI 10.1016/S0921-5093(00)01810-4.
17. Pichaimani, P., Krishnan, S., Song, J. K., Muthukaruppan, A. (2019). Bio-silicon reinforced siloxane core polyimide green nanocomposite with multifunctional behavior. *High Performance Polymers*, 30(5), 549–560. DOI 10.1177/0954008317709891.
18. Moustafa, H., Darwish, N. A., Nour, M. A., Youssef, A. M. (2018). Biodegradable date stones filler for enhancing mechanical, dynamic, and flame retardant properties of polyamide-6 biocomposites. *Polymer Composites*, 6, 1978–1987. DOI 10.1002/pc.24157.
19. Moustafa, H., Youssef, A. M., Nour, M. A. (2016). Investigation of morphology, mechanical, thermal and flame retardant properties of an EVA/EPDM blend by combination of organoclay with Na⁺-tripolyphosphate. *RSC Advances*, 43, 36467–36474. DOI 10.1039/C6RA03341E.
20. Dul, S., Fambri, L., Pegoretti, A. (2016). Fused deposition modelling with ABS-graphene nanocomposites. *Composites Part A: Applied Science and Manufacturing*, 85, 181–191. DOI 10.1016/j.compositesa.2016.03.013.
21. Pedrazzoli, D., Pegoretti, A. (2014). Expanded graphite nanoplatelets as coupling agents in glass fiber reinforced polypropylene composites. *Composites Part A: Applied Science and Manufacturing*, 66, 25–34. DOI 10.1016/j.compositesa.2014.06.016.
22. Postiglione, G., Natale, G., Griffini, G., Levi, M., Turri, S. et al. (2015). Conductive 3D microstructures by direct 3D printing of polymer/carbon nanotube nanocomposites via liquid deposition modeling. *Composites Part A: Applied Science and Manufacturing*, 76, 110–114. DOI 10.1016/j.compositesa.2015.05.014.
23. Compton, B. G., Lewis, J. A. (2014). 3D-printing of lightweight cellular composites. *Advanced Materials*, 26(34), 5930–5935. DOI 10.1002/adma.201401804.
24. Tang, J., Mu, B., Zong, L., Wang, A. (2019). From waste hot-pot oil as carbon precursor to development of recyclable attapulgite/carbon composites for wastewater treatment. *Journal of Environmental Sciences*, 75, 346–358. DOI 10.1016/j.jes.2018.05.014.
25. Dong, S., Li, B., Zhang, J., Wang, A. (2018). Superamphiphobic coatings with low sliding angles from attapulgite/composites. *Advanced Materials Interfaces*, 5(9), 1701520. DOI 10.1002/admi.201701520.

26. Tian, G., Wang, W., Mu, B., Kang, Y., Wang, A. et al. (2016). Ag(I)-triggered one-pot synthesis of Ag nanoparticles onto natural nanorods as a multifunctional nanocomposite for efficient catalysis and adsorption. *Journal of Colloid and Interface Science*, 473, 84–92. DOI 10.1016/j.jcis.2016.03.058.
27. Wang, L., Sheng, J. (2005). Preparation and properties of polypropylene/org-attapulgite nanocomposites. *Polymer*, 46(16), 6243–6249. DOI 10.1016/j.polymer.2005.05.067.
28. Wang, L., Sheng, J. (2003). Graft polymerization and characterization of butyl acrylate onto silane-modified attapulgite. *Journal of Macromolecular Science, Part A*, 40(11), 1135–1146. DOI 10.1081/MA-120024829.
29. Tian, M., Cheng, L., Liang, W., Zhang, L. (2005). The anisotropy of fibrillar silicate/rubber nanocomposites. *Macromolecular Materials & Engineering*, 290(7), 681–687. DOI 10.1002/mame.200400400.
30. Unal, H. (2004). Morphology and mechanical properties of composites based on polyamide 6 and mineral additives. *Materials & Design*, 25(6), 483–487. DOI 10.1016/j.matdes.2004.01.007.
31. Riccò, T., Pavan, A., Danusso, F. (1975). Dynamic transition of grafted polybutadiene in ABS resins. *Polymer*, 16 (9), 685–689. DOI 10.1016/0032-3861(75)90077-4.
32. Más, J., Vidaurre, A., Meseguer, J. M., Romero, F., Monleón Pradas, M. et al. (2002). Dynamic mechanical properties of polycarbonate and acrylonitrile–butadiene–styrene copolymer blends. *Journal of Applied Polymer Science*, 83(7), 1507–1516. DOI 10.1002/app.10043.
33. Sepe, M. (1998). *Dynamic mechanical analysis for plastics engineering*. Norwich, New York: Plastics Design Library.
34. Tiganis, B. E., Burn, L. S., Davis, P., Hill, A. J. (2002). Thermal degradation of acrylonitrile–butadiene–styrene (ABS) blends. *Polymer Degradation & Stability*, 76(3), 425–434. DOI 10.1016/S0141-3910(02)00045-9.